Registry No. **1**, 99589-88-5; **2**, 136762-71-5; **3a**, 136762-72-6; **3a**·MeCN, 136762-75-9; **3b**, 136762-73-7; **3b**·THF, 136762-76-0; **3c**, 136762-74-8; **4**, 14989-38-9; $NSiMe_3^{2-}$, 136379-30-1.

Supplementary Material Available: Text giving characterization data for compounds **2** and **3a-c** and X-ray crystal data for **3a** including text describing the experimental procedures, an ORTEP drawing showing all non-hydrogen atoms, and tables of crystal data, atomic coordinates and equivalent isotropic displacement coefficients, interatomic distances, interatomic angles, anisotropic displacement coefficients, hydrogen atom coordinates, and isotropic displacement coefficients (14 pages); a listing of observed and calculated structure factors (26 pages). Ordering information is given on any current masthead page.

Department of Chemistry
University of Washington
Seattle, Washington 98195
Beth M. Schomber

Department of Chemistry
University of California
Irvine, California, 92717
Joseph W. Ziller
Nancy M. Doherty*

Received July 30, 1991

Articles

Contribution from the Laboratoire de Physique Quantique, URA 505 du CNRS, and Laboratoire de Chimie Inorganique, Université Paul Sabatier, 205 Route de Narbonne, F-31077 Toulouse Cedex, France, and Laboratoire de Chimie Quantique, UPR 139 du CNRS, Université Louis Pasteur, 4 Rue B. Pascal, F-67000 Strasbourg, France

$Ni_2Cl_2[C(SiMe_3)(PMe_3)]_2$, Containing a Very Short Ni-Ni Distance with Little Metal-Metal Bonding Character: Possible Synergy of Electronic and Steric Factors

Georges Trinquier,[†] Michèle Dartiguenave,[‡] Yves Dartiguenave,[‡] and Marc Bénard*[,§]

Received March 15, 1991

The electronic structure of the title compound, a recently characterized dimer of nickel(II), is investigated by means of extended Hückel calculations. In contradiction with early predictions based upon electron counting and structural considerations, the very short nickel-nickel distance (2.281 Å) does not appear to be the consequence of strong metal-metal bonding interactions. The origin of the rhombic conformation of the Ni_2C_2 metallacycle is then traced to the interactions that develop between the Ni_2Cl_2 fragment and the bridging ylide moieties, ensuring a tight nickel-carbon binding. Electronic effects alone do not seem to be sufficient to account for the very short Ni-Ni distance. H···H repulsive contacts that develop between the bulky substituents of the bridging ylides also tend to displace the equilibrium conformation toward shorter metal-metal distances. Ab initio calculations carried out on appropriate model systems indicate that the repulsive part of the H···H interaction energy could amount to 66 kJ·mol^{-1} for the title complex at the equilibrium conformation and reach 125 kJ·mol^{-1} in a hypothetical "square" conformation of the metallacycle corresponding to a Ni-Ni distance of 2.695 Å.

1. Introduction

The structure of a novel binuclear complex of nickel(II) with two symmetrically bridging ylide ligands has recently been reported.[1] $Ni_2Cl_2[C(SiMe_3)(PMe_3)]_2$ (**1**) is a dimer with C_{2h} symmetry (Figure 1) characterized by an extremely short metal-metal bond length (2.281 Å), which is the shortest distance reported for binuclear Ni complexes. The angles in the Ni_2C_2 planar metallacycle are Ni-C-Ni = 73.5° and C-Ni-C = 106.5°. These structural characters were first interpreted as supporting the presence of a strong Ni-Ni bonding interaction. This appears to be in agreement with formal electron counting considerations that require a double metal-metal interaction in order to achieve a 16e environment around each nickel atom.[1]

We first carried out extended Hückel calculations on the model dimer $Ni_2Cl_2[C(SiH_3)(PH_3)]_2$ (**2**) in order to confirm the presence of the assumed metal-metal double bond. To our surprise, the calculations did not clearly corroborate the existence of a strong Ni-Ni bonding interaction. We therefore decided to carry out a more thorough investigation of the factors leading to such a short metal-metal bond. Most of the present work relies on extended Hückel (EH) calculations,[2] but a quantitative assessment of the steric effects was carried out through ab initio SCF calculations.

2. Computational Details

The orbital exponents and H_{ii}'s used for the EH calculations are listed in Table I. The EH calculations on the model system **2** were carried out using for the non-hydrogen skeleton the geometry corresponding to the X-ray structure of the real complex.[1] P-H distances of 1.42 Å and Si-H distances of 1.48 Å were then assumed, with C-Si-H and C-P-H angles of 109.47°. The metallacycle was then distorted from the experimental rhombus to a square shape corresponding to Ni-Ni and C···C distances of 2.695 Å. The Ni-C distances and all other geometrical parameters were kept constant. The molecule therefore retains the C_{2h} symmetry along the deformation path. Different sets of EH parameters had been used for Ni, Cl, and Si in preliminary calculations without

Table I. Extended Hückel Parameters

atom	orbital	H_{ii}, eV	ζ
Ni	4s	-6.86	2.10
	4p	-4.90	2.10
	3d	-12.99	5.49 (0.563 36)[a]
			2.00 (0.620 95)
C	2s	-21.40	1.625
	2p	-11.40	1.625
Si	3s	-17.30	1.383
	3p	-9.20	1.383
P	3s	-18.60	1.60
	3p	-14.00	1.60
Cl	3s	-30.00	2.033
	3p	-15.00	2.033
H	1s	-13.60	1.30

[a] Contraction coefficients used in the double-ζ expansion.

[†] Laboratoire de Physique Quantique, Université Paul Sabatier.
[‡] Laboratoire de Chimie Inorganique, Université Paul Sabatier.
[§] Laboratoire de Chimie Quantique, Université Louis Pasteur.

(1) König, H.; Menu, M. J.; Dartiguenave, M.; Dartiguenave, Y.; Klein, H. F. *J. Am. Chem. Soc.* **1990**, *112*, 5351.
(2) (a) Hoffmann, R. *J. Chem. Phys.* **1963**, *39*, 1397. (b) Hoffmann, R.; Lipscomb, W. N. *Ibid.* **1962**, *36*, 2179; **1962**, *37*, 2872.

0020-1669/91/1330-4490$02.50/0

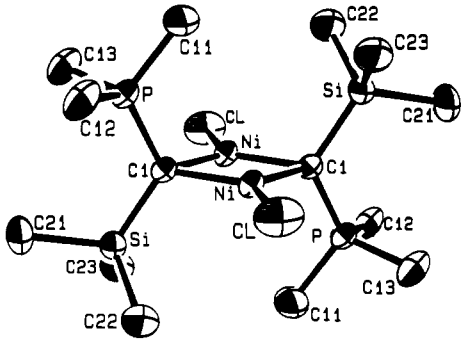

Figure 1. Crystal structure of **1** (ORTEP plot, thermal ellipsoids at 50%, without H atoms).

modifying the interpretation of the interaction diagrams.

Ab initio SCF calculations were also carried out on the model systems PH_3, $(PH_3)_2$, $P(CH_3)_3$, and $[P(CH_3)_3]_2$ in order to assess the order of magnitude of the repulsive part of the H···H interaction energy between two bulky substituents in the real complex. The results were corrected from the basis set superposition error (BSSE) using the counterpoise method proposed by Boys and Bernardi.[3] Details about the choice of the model and the geometry of the interacting fragments are given in section 4.2. The calculations were carried out with the ASTERIX program system.[4] The basis sets were (11, 7) contracted into [4, 3] for phosphorus and (4) contracted into [2] for hydrogen.[5]

3. Results and Discussion

Let us first consider complex **2** as an assembly of interacting fragments. The most convenient decomposition scheme leads to the interaction of two fragment dimers, a metallic fragment $[NiCl]_2^{2+}$ and a combination of the two bridging ligands $[C(PH_2)(SiH_3)]_2^{2-}$. If the nickel is to be considered in oxidation state II as it was in the first experimental report, then each bridging ligand must be attributed a −1 charge. The zwitterionic nature of the ylide ligand should then be formally accounted for by assigning a +1 charge to the phosphorus and a −2 charge to the carbon atom that becomes a four-electron donor.

The frontier orbitals of the metallic fragment resulting from the coupling of two $[NiCl]^+$ monomers are displayed in Figure 2 for the Ni–Ni bond lengths corresponding to both the "rhombic" (d_{Ni-Ni} = 2.28 Å; left-hand side of Figure 2) and the "square" (d_{Ni-Ni} = 2.695 Å; right-hand side) conformations. The electronic configurations of Ni(II) being d^8, the metal valence orbitals are occupied with 16 electrons. The ground-state electronic configuration is $\pi^4\delta^4\sigma^2\delta^{*4}\pi^{*2}$, corresponding to a metal–metal double bond. Note that the d_{z^2} orbital of the $[NiCl]^+$ monomer is pushed up in energy because of the σ donation from Cl^-. This energy shift of the d_{z^2} orbital explains why the stabilized σ-bonding orbital of the dimer lies slightly above the degenerate δ^* orbitals. Both the σ and the σ^* orbitals are antibonding with respect to the strong Ni–Cl interaction. A contribution from the metal 4s orbital combination with appropriate symmetry reduces this antibonding character (and also the metal–metal antibonding character of the σ^* orbital) by deflating the lobes of the d_{z^2} orbitals to the benefit of the density ring. An effect of this 4s admixture is therefore to reduce the metal–metal σ overlap, thus explaining why the σ–σ^* energy gap becomes slightly smaller than the π–π^* gap in the experimental conformation. As another consequence of the 4s admixture, the σ and the σ^* fragment orbitals are relatively insensitive to the variations of the metal–metal distance. This is at variance from the π and π^* levels, strongly affected by the stretching of the metal–metal bond (Figure 2).

The orbitals of the ligand dimer represented in Figure 3 are symmetry-adapted combinations of the frontier orbitals of the $[C(PH_3)(SiH_3)]^-$ moieties, ready to interact with those of the

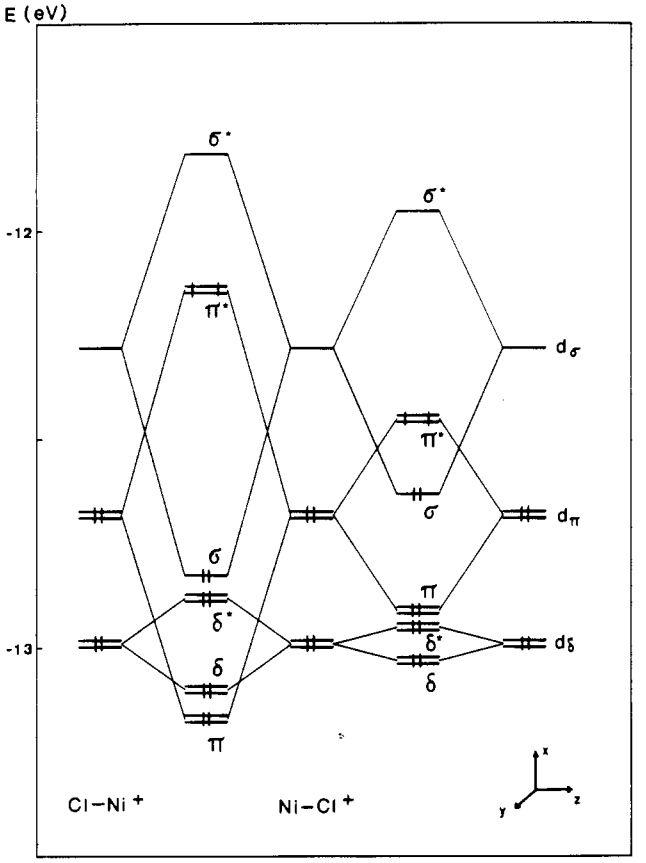

Figure 2. Interaction diagram leading to the EH orbitals of the $[Ni_2Cl_2]^{2+}$ fragment: Left-hand side, d_{Ni-Ni} = 2.281 Å (rhombic conformation of **2**); right-hand side, d_{Ni-Ni} = 2.695 Å ("square" conformation of **2**).

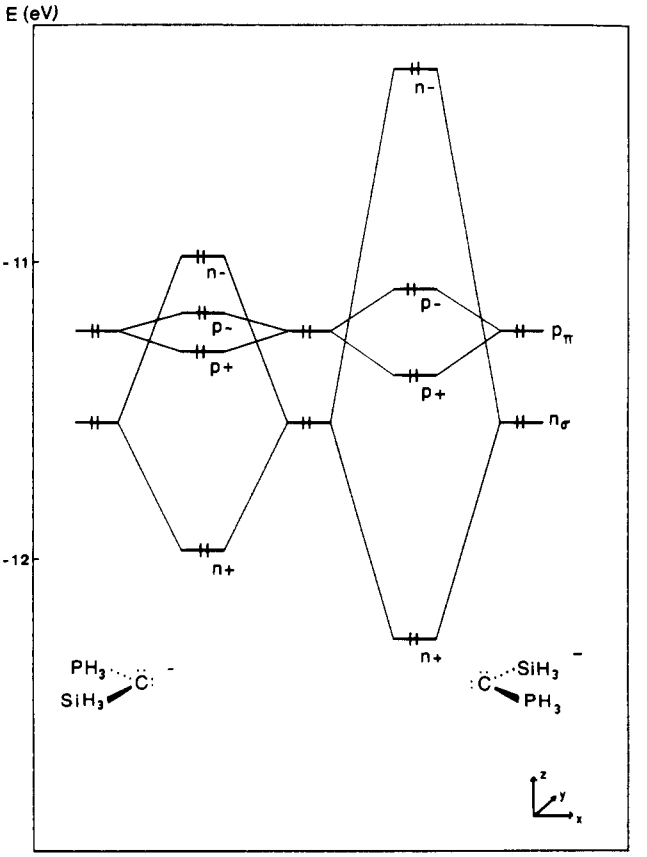

Figure 3. Interaction diagram leading to the EH orbitals of the $[CSiH_3PH_3]_2^{2-}$ fragment: Left-hand side, $d_{C\cdots C}$ = 3.05 Å; right-hand side, $d_{C\cdots C}$ = 2.695 Å.

(3) Boys, S. F.; Bernardi, F. *Mol. Phys.* **1970**, *19*, 553.
(4) (a) Ernenwein, R.; Rohmer, M.-M.; Bénard, M. *Comp. Phys. Commun.* **1990**, *58*, 305. (b) Rohmer, M.-M.; Demuynck, J.; Bénard, M.; Wiest, R.; Bachmann, C.; Henriet, C.; Ernenwein, R. *Ibid.* **1990**, *60*, 127.
(5) Huzinaga, S. Technical Report. University of Alberta, Edmonton, Canada, 1971.

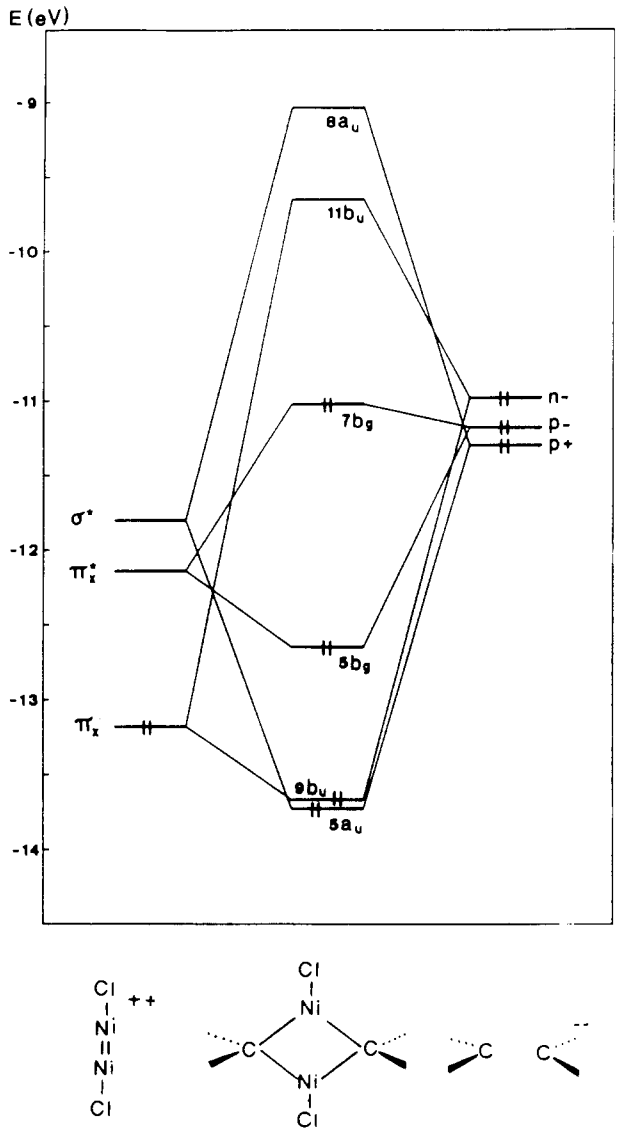

Figure 4. Simplified interaction diagram (from EH calculations) displaying the Ni–C interactions in the rhombic conformation of **2** (d_{Ni-Ni} = 2.281 Å).

metallic fragment. Each $[C(PH_3)(SiH_3)]^-$ monomer is isoelectronic with a dianionic carbene bearing two lone pairs corresponding to occupied n_σ and p_π orbitals. A convenient way for depicting this entity is to start from a regular phosphonium ylide and then to deprotonate the $CH(SiH_3)$ part (**3**). The ylilic and

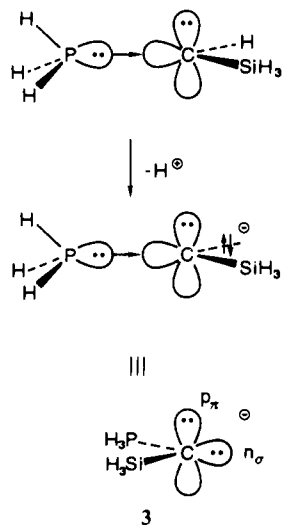

3

carbene characters of the fragment hence appear clearly, characterized by two doubly occupied orbitals n_σ (−11.54 eV) and p_π (−11.23 eV). Combining the two monomers leads to a splitting of the n_σ and p_π orbitals into bonding and antibonding doubly occupied combinations, respectively, labeled n+, n−, p+, and p−, as indicated in Figure 3 for both the experimental rhombic conformation (left-hand side) and the hypothetic "square" conformation (right-hand side). Even though the two carbon atoms are pretty far apart in the rhombic conformation (3.05 Å), the n+/n− splitting reaches 1 eV, since the two n_σ orbitals point toward each other. At such distance, the π interaction is weak and the p+/p− separation is quite small. It should be noticed that no acceptor ligand orbital is available. In the present scheme, the ligand–metal bond in the complex will therefore be effective through ligand-to-metal donation with negligible metal-to-ligand back-donation.

A complete interaction diagram between the valence orbitals of the fragment dimer giving rise to complex **2** would involve 36 occupied orbitals and 26 virtual orbitals. In a first approach to delineate the electronic structure of the metallacycle, we will restrict the interaction diagram to those interactions giving rise to the metal–metal and metal–carbon couplings. Since the four ligand orbitals lie in the Ni_2C_2 plane (xz plane), all metal orbitals antisymmetric with respect to this plane, namely the δ,δ^* combinations of the d_{xy} orbitals and the π_y,π_y^* combinations of the d_{yz} orbitals, will basically remain free from ligand contamination. Ligand interaction with the in-plane metal combinations will break the orbital degeneracy of the linear fragment, and the two electrons populating the π^* levels (Figure 2) are transferred to the final complex through the unperturbed π_y^* orbital. Some other interactions will also be put aside in this first overview, since they result in four-electron repulsive interactions that cannot contribute to the metal–ligand bonding. This eliminates the δ and δ^* combinations of the $d_{x^2-y^2}$ orbitals, which respectively mix with n+ in the A_g representation and with p+ in the A_u representation. The metal σ orbital also takes part in a repulsive interaction with n+ in the A_g representation. We are then left with an interaction diagram involving six fragment orbitals, namely the π_x, π_x^* and σ^* orbitals of the $[Ni_2Cl_2]^{2+}$ fragment and the p+, p−, and n− orbitals of the ligand dimer (Figure 4). Since the two π^* electrons of the dimetal fragment are accommodated in the unperturbed π_y^* orbital (not displayed in Figure 4), the interacting orbitals are populated altogether with 8 electrons, 6 of them originating in ligand orbitals.

Those fragment orbitals give rise to three important interactions. The interaction of π_x with n− gives rise to the bonding Ni–C combination $9b_u$ (**4**). Orbital $9b_u$ is stabilized by no more than

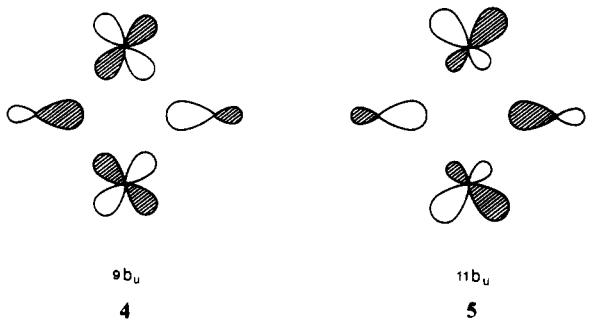

4 **5**

0.5 eV with respect to the π_x level, but underlying 4-electron interactions involving $9b_u$ and $10b_u$ as the upper terms convey an important part of the stabilization to low-lying orbitals, especially $8b_u$ (Figure 5). If we return to Figure 4, the upper term of the interaction in the B_u symmetry, orbital $11b_u$ (**5**), is largely destabilized. Even though the interacting fragment orbitals are both occupied, orbital $11b_u$ happens to be the LUMO of the complex, by virtue of the aufbau principle. Let us note that this *unoccupied* level carries an important metal contribution (54%) with Ni–Ni *bonding* character.

Another strongly bonding metal–ligand interaction involves the metal σ^* combination and the ligand orbital with proper symmetry, p+. This interaction involves a secondary mixing with the $\delta_{x^2-y^2}^*$

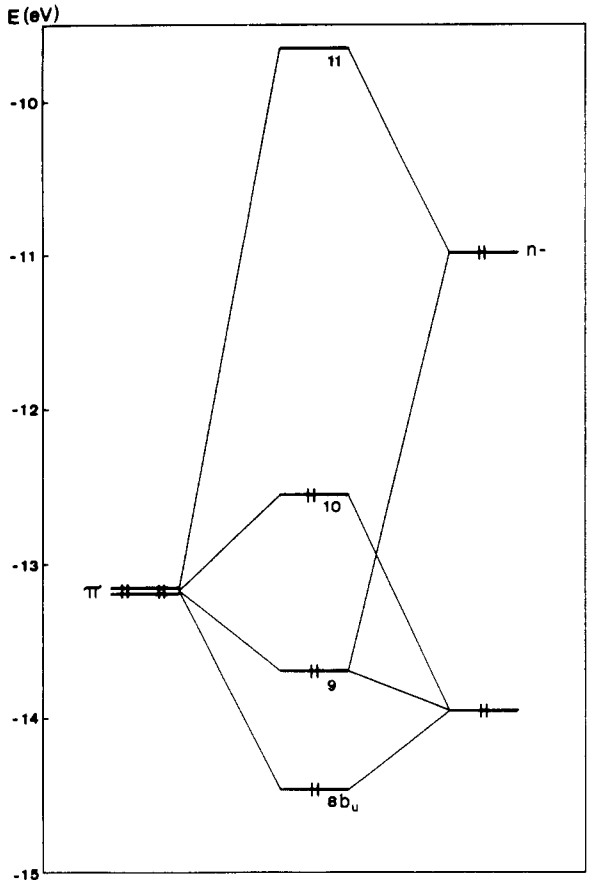

Figure 5. Interaction diagram (from EH calculations) displaying the frontier orbitals of **2** in the B_u representation.

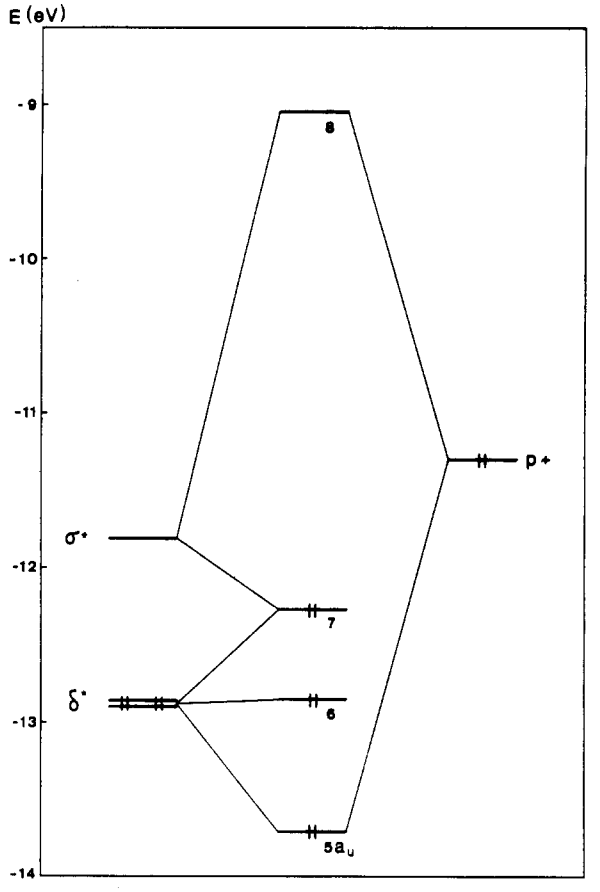

Figure 6. Interaction diagram (from EH calculations) displaying the frontier orbitals of **2** in the A_u representation.

level of the metal fragment (Figure 6), so that the stabilized orbital, $5a_u$ (**6**), retains a large metal weight (57%) with out-

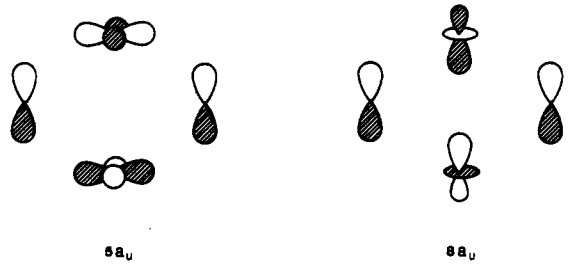

6 **7**

of-phase $d_{x^2-y^2}$ character. The destabilized counterpart of this interaction, $8a_u$ (**7**), is both metal–ligand and metal–metal antibonding, with 48% metal character.

Finally, π_x^* mixes with p– in the B_g representation. The in-phase combination, $5b_g$ (**8**) is stabilized by 0.5 eV with respect

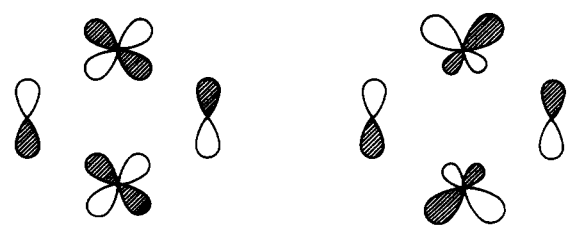

8 **9**

to the interacting level of the metal fragment. The out-of-phase combination $7b_g$ should be metal–metal antibonding and strongly destabilized. A secondary mixing occurs however with the out-of-phase combination of the metal p_x orbitals, leading to orbital **9**. The lobes of the d_{xz} orbitals internal to the metal–metal axes are reduced in **9**, thus decreasing the metal–ligand antibonding character. Some metal–carbon *bonding* character could even develop through the outer lobes of the metal dp hybrids. As a matter of fact, the $7b_g$ orbital is scarcely destabilized with respect to p– and becomes the HOMO of the complex at –11.02 eV. Even though the interaction giving rise to $5b_b/7b_g$ happens to be a four-electron metal–ligand interaction by virtue of the aufbau principle, the contribution of the metal $4p_x$ combination makes the interaction globally bonding *at the experimental conformation.* It will be shown below that the 4-electron interaction gains strength when the metallacycle is distorted toward a square conformation, the energy of the HOMO increasing steadily with the metal–metal distance. At the observed geometry, however, the HOMO has a relatively low energy and the HOMO–LUMO gap is reasonably large (1.4 eV), ensuring the complex a good kinetic stability.

In conclusion, three major interactions between the $[Ni_2Cl_2]^{2+}$ and the $[C(SiH_3)(PH_3)]_2^{2-}$ fragments contribute to strengthen the metal–carbon bonds. This results in a tightly bound complex, as appears from the short Ni–C distance (1.906 Å) obtained from the crystal structure. One should notice that this tight binding extends to the NiCl bond, also characterized by a very short distance (2.143 Å). A strong Ni–Cl bond pushes up the energy of the metal d_σ orbital, and the same shift is transmitted to the σ and σ^* levels in the $[Ni_2Cl_2]^{2+}$ dimer (Figure 2). Figure 4 shows that this rise of the σ^* orbital maximizes the strength of the $5a_u/8a_u$ stabilizing interaction by reducing the energy gap between σ^* and the high-lying ligand orbital of the same symmetry, p+. It also comes out from the diagram of Figure 4 that the electronic structure of the complex is completely conditioned by the metal–ligand stabilizing interactions, the metal–metal character of the resulting orbitals seeming to contribute no more than as a side effect. The metal–metal σ-bonding character present in the $[Ni_2Cl_2]^{2+}$ fragment is retained in the complex, in spite of a 4-electron interaction between the σ orbital and the ligand n+ level. However, a consequence of the strong interaction occurring in the a_u representation (Figures 4 and 6) is to bring back into

the occupied set a large contribution from the metal–metal σ^* combination. Because of the secondary mixing with the δ^* occupied orbital, this contribution, about 50%, is distributed between orbitals $5a_u$ and $7a_u$. The σ contribution to the metal–metal bond order should therefore be approximated as $+1.0 - 0.5 = +0.5$ only. The Mulliken population of the d_{z^2} metal orbital, 1.55 e, is consistent with this appraisal.

Still more unexpected is the behavior of the metal–metal π_x bonding orbital, split into one occupied orbital ($9b_u$) and one unoccupied MO ($11b_u$) (Figure 4). The metal weight of the LUMO (54%, including some contamination from the metal p_x out-of-phase combination) indicates that an important part of the π_x bonding character has been lost for the complex, whereas, in the b_g representation, all of the π_x^* character is distributed between the $5b_g$ and $7b_g$ orbitals, both occupied. Since both π_y and π_y^* remain doubly occupied, the net π contribution to the metal–metal bond order happens to be negative and should be assessed in the first approximation to be −0.5. The computed d_{xz} population, 1.60 e, suggests that this approximation probably represents a lower bound. The other metal orbitals have populations close to 2 electrons ($d_{x^2-y^2}$, 1.85 e; d_{xy}, 1.99 e; d_{yz}, 1.99 e), indicative of little contribution if any to the metal–metal bond order. *In the first approximation, the Ni–Ni bond order should therefore be zero* or just slightly positive accounting for the probable overestimation of the negative π_x^* contribution. This analysis is comforted by the value of +0.13,[6] positive, but rather low, obtained for the Ni–Ni overlap population, compared to the value of +0.29 obtained for the metal–metal double bond of the $[Ni_2Cl_2]^{2+}$ fragment.

This relative unimportance of the metal–metal interactions in the stability of complex **1** seems to support the thesis of Gambarotta et al.[7] according to which the metal–metal distance in binuclear complexes is conditioned by metal–ligand interactions. The case of complex **1** is particularly puzzling, however, because of the following considerations: (i) This molecule with little metal–metal bonding interaction displays the shortest Ni–Ni distance ever reported for binuclear complexes of nickel. (ii) The short M–M distance cannot be considered only as a consequence of the tight Ni–C binding of the metallacycle, since the rhombic distortion of the metallacycle (Ni–C–Ni = 73.5°) suggests a strong Ni–Ni bonding interaction. (iii) The lack of a net metal–metal bonding interaction makes the complex largely unsaturated with an electron surrounding of only 14 e around each nickel. (iv) Finally, the large donation from the ylide ligands to the metal atoms, leading to the complete occupation of both the π_x^* and the π_y^* orbitals, questions the assignment of the metal as Ni(II). Although this point is purely formal and does not affect the interaction diagram, neutral, three-electron donor ylide ligands acting on Ni(I) might more adequately reflect the electronic structure of the complex.

In order to elucidate those problems and more specifically to trace the origin of the short Ni–Ni bond, we have analyzed the electronic and steric effects of an angular deformation of the Ni_2C_2 metallacycle from the observed rhombus to a hypothetical square conformation. The Ni–C distance (1.906 Å) and all other geometrical parameters are kept constant along the deformation path, and the square conformation is characterized by the Ni–Ni and C···C distances being equal at 2.695 Å. The electronic effects will be discussed from Walsh diagrams obtained for the model molecule **2** for which the steric strain is expected to be negligible. A tentative assessment of the steric effects in molecule **1** will then be carried out through ab initio SCF calculations.

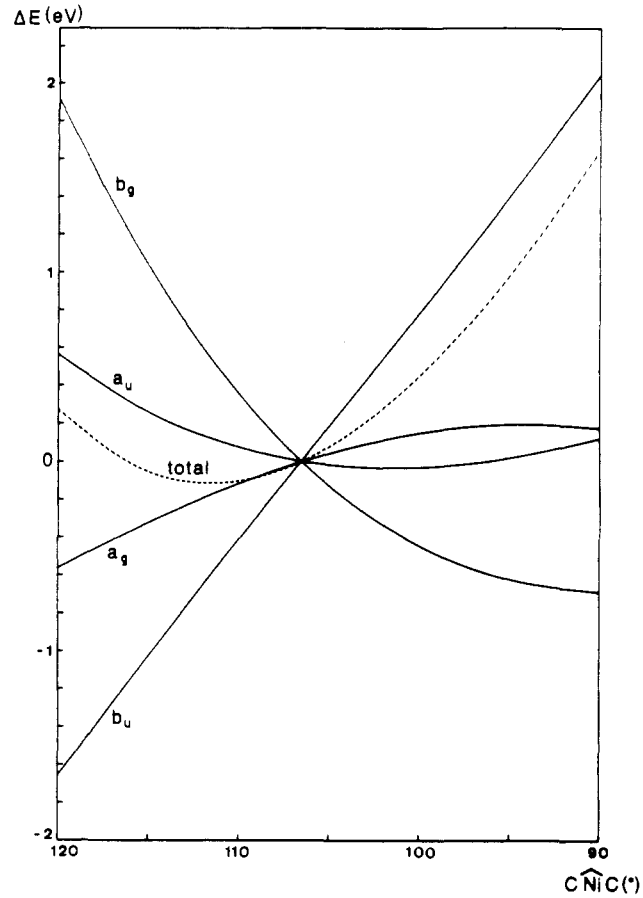

Figure 7. Potential energy curves (from EH calculations on model complex **2**) representing the variation of the total energy (dotted line) and of the energies associated with each irreducible representation of the C_{2h} point group (solid lines) as functions of the C–Ni–C angle. Energies are in eV, with the zero-point energy corresponding to the energy of the observed structure of **1**.

4. Deformation of the Metallacycle

4.1. Electronic Effects. Figure 7 displays (dotted lines) the potential energy curves obtained for the model system **2** by varying the C–Ni–C angle from 90° ("square" conformation) to 120°. The experimental conformation (106.5°) is pointed out as the zero-energy point. The minimum is obtained for C–Ni–C ~ 112°, that is at a Ni–Ni distance *shorter* than the experimental value. Although such an optimization carried out at the EH level cannot be considered as quantitatively reliable, it shows that, in spite of the weak Ni–Ni bonding interactions, electronic effects are at work that favor the rhombus conformation with a short metal–metal distance. In the same Figure 7 is displayed a decomposition of the total energy into four contributions associated each with an irreducible representation of the C_{2h} point group. The evolution of the most representative frontier orbitals is displayed in Figure 8 and discussed as follows:

A_g Representation. The fragment orbitals of $[Ni_2Cl_2]^{2+}$, σ and $\delta_{x^2-y^2}$, are metal–metal bonding. Both are destabilized when the Ni–Ni distance increases, that is when going toward the "square" conformation. This destabilization is transferred to the resulting MO with major metal character, $12a_g$, destabilized by 0.30 eV with respect to the experimental conformation. On the opposite way, the ligand in-phase a_g combination, n+, is *stabilized* by a similar amount when the two carbons are approaching each other, and this stabilization is transferred to the underlying a_g orbitals of the complex. The global effect is no more than slightly favorable to the experimental conformation (Figure 7).

(6) This positive value also accounts for the σ overlap being larger than the π one. The positive contribution of the σ "half-bond" prevails over the negative contribution of the π_x^* "half-antibond". Other positive contributions arising from secondary mixings also raise the overlap population value. Let us mention the most important one, arising from a contribution of the in-phase $4p_z$ combination to the $12a_g$ and $11a_g$ σ-bonding orbitals.

(7) (a) Edema, J. J. H.; Gambarotta, S.; Spek, A. L. *Inorg. Chem.* **1989**, *28*, 812. (b) Edema, J. J. H.; Gambarotta, S.; van Bolhuis, F.; Smeets, W. J. J.; Spek, A. L. *Ibid.* **1989**, *28*, 1407. (c) Edema, J. J. H.; Gambarotta, S.; van der Sluis, P.; Smeets, W. J. J.; Spek, A. L. *Ibid.* **1989**, *28*, 3784. (d) Edema, J. J. H.; Gambarotta, S.; van Bolhuis, F.; Spek, A. L. *J. Am. Chem. Soc.* **1989**, *111*, 2142. (e) Edema, J. J. H.; Gambarotta, S.; Meetsma, A.; van Bolhuis, F.; Spek, A. L.; Smeets, W. J. J. *Inorg. Chem.* **1990**, *29*, 2147.

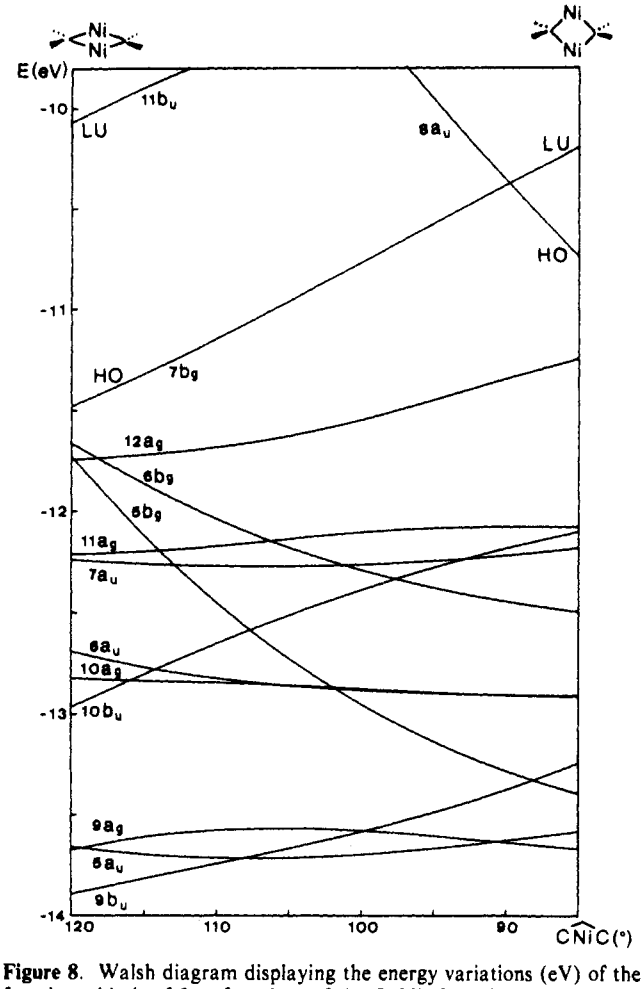

Figure 8. Walsh diagram displaying the energy variations (eV) of the frontier orbitals of **2** as functions of the C–Ni–C angle.

A_u Representation. All interacting fragment orbitals (σ^* and δ^* for the dimetal fragment, p+ for the ligand dimer) are slightly stabilized in the square conformation. Metal–ligand overlap decreases however with the C–Ni–C angle (see **6** and **7**), thus reducing the energy splitting between $5a_u$ and $8a_u$ (Figure 6). For $5a_u$ (**6**), the weakening of the interactions just offsets the energy lowering of the interacting levels, and the energy contribution of the a_u representation remains balanced between 90 and 110°. By contrast, the stabilization of the unoccupied out-of-phase combination $8a_u$ (**7**) is impressive (~1 eV). This MO becomes the LUMO of the square conformation and even crosses the HOMO level $7b_g$ when the C–Ni–C angle approaches 90°.

B_g Representation. The orbitals of the metal fragment belonging to this representation are the π^* combination, stabilized by ~0.35 eV in the square conformation. The out-of-plane π_{yz}^* molecular orbital ($6b_g$), unaffected by ligand interactions, retains this stabilization. The other π^* orbital is involved in a 4-electron interaction with the p– ligand combination. The metal–ligand π overlap is improved in the square conformation, thus strengthening the 4-electron interaction. This clearly appears in the widening of the energy gap between $5b_g$ and $7b_g$ (**8** and **9**) while decreasing the C–Ni–C angle (Figure 8). As the system evolves toward the square conformation, the destabilization due to the 4-electron interaction progressively offsets the stabilization of the π^* metal fragment orbitals. These opposite effects are evidenced in the curve displaying the B_g contribution to the valence energy (Figure 7). The energy decrease remains steep when C–Ni–C is varying from 120 to 105°, that is when the energy variation is dominated by the stabilization of the fragment orbitals. Beyond 105°, the destabilizing interaction becomes more and more sensible and makes the decrease of the B_g energy contribution progressively more shallow (Figure 7).

B_u Representation. Both the metal π and the ligand n– fragment combinations are strongly destabilized in the square conformation, respectively by 0.25 and 0.40 eV (Figures 2 and 3). The interactions remain as described in Figure 4, but all frontier orbitals $9b_u$–$11b_u$ including the metal out-of-plane π-level $10b_u$ are shifted up by ~0.3 eV. Underlying levels are also shifted up by smaller amounts. The result is a steep and steady increase of the B_u contribution from C–Ni–C = 120 to 90°. Between 110 and 90°, this destabilization of the b_u orbitals conditions the evolution of the total energy.

To summarize, the evolution of the total energy of **2** when the C–Ni–C angle is varied should be traced first to the energy changes in the *fragment* orbitals and more specifically in the σ, σ^*, π, and π^* orbitals of the $[Ni_2Cl_2]^{2+}$ fragment. It has been noticed in section 3 that the admixture of the low-lying 4s orbital was at the origin of a relative insensitivity of the σ and more especially σ^* fragment orbitals levels to the Ni–Ni distance. These small displacements of the fragment level energies explain in part the near constancy of the A_u and A_g contributions to the energy for C–Ni–C varying between 105 and 90°. The wider energy variations in opposite directions of the π and π^* fragment orbitals are at the origin of the B_g and B_u contributions.[8] The key point displacing the equilibrium toward short Ni–Ni distances appears to be the destabilizing interaction between the metal π^* and the ligand p– combinations, which yield the molecular orbitals $5b_g$ and $7b_g$. The rise of the metal–ligand overlap when the square conformation of the metallacycle is approached strengthens the 4-electron interaction, thus preventing any stretching of the metal–metal distance. The steady rise of the HOMO energy with the Ni–Ni distance, in spite of its metal–metal antibonding character, illustrates this point. In a paradox that is not uncommon in the field of dimetal complexes, the removal of two electrons would simultaneously increase the metal–metal bond order and displace the equilibrium conformation toward a larger metal–metal distance. An example of such a displacement could be provided by the series of amide-bridged dimers $[M(NPh_2)_2]_2$, with M = Ni, Co, and Fe. In the amide-bridged dimer of Ni(II),[9] the structure of the Ni_2N_2 metallacycle is quite similar to that of the Ni_2C_2 core in **1**, with a very short Ni–Ni distance of 2.327 Å and a Ni–Ni angle of 75.0°. Extended Hückel calculations on $[Ni(NH_2)_2]_2$ show that the two highest occupied and the two lowest unoccupied orbitals of this model complex are quite similar to those of **1** displayed in Figure 8. Then, the replacement of Ni by Co should remove the two electrons from the HOMO $7b_g$ and favor a conformation with a longer metal–metal bond (Figure 8). This trend is indeed verified, since the observed M–M bond length in the cobalt dimer is 2.556 Å and the Co–Ni–Co angle reaches 79.9°.[9] Removing two more electrons would empty the metal–metal σ-bonding orbital $12a_g$ and further distort the metallacycle toward a square conformation, as observed in $[Fe(NPh_2)_2]_2$ (d_{Fe-Fe} = 2.715 Å; Fe–N–Fe = 83.6°).[10] Similar Co–Co and Fe–Fe distances are observed in $[M\{N(SiMe_3)_2\}_2]_2$ (d_{Co-Co} = 2.583 Å;[11] d_{Fe-Fe} = 2.663 Å[10]).

Let us finally remind that the Ni–Ni overlap population at the experimental geometry is small but not negligible (+0.13) and that it is steadily decreasing with the C–Ni–C angle (+0.06 at 90°). This trend is not unexpected in view of the rapidly vanishing 3d–3d overlap.

The present analysis might explain why the Ni–Ni distance in **1** should be short enough to suggest the presence of a metal–metal bond, even though this bond is almost elusive. It still remains as a paradox, however, that this dimetal complex, which such small net metal–metal bonding, displays the shortest known Ni–Ni bond. Another effect could be at work, acting in synergy with the electronic interactions. We therefore investigated the influence of the steric crowding induced by the bulky substituents of **1**.

(8) The presence of *degenerate* π and π^* levels, both shifted in the Ni_2Cl_2 fragment, obviously contributes to magnify the energy variations in the B_g and B_u representations.

(9) Hope, H.; Olmstead, M. M.; Murray, B. D.; Power, P. P. *J. Am. Chem. Soc.* **1985**, *107*, 712.
(10) Olmstead, M. M.; Power, P. P.; Shoner, S. C. *Inorg. Chem.* **1991**, *30*, 2547.
(11) Murray, B. D.; Power, P. P. *Inorg. Chem.* **1984**, *23*, 4584.

Table II. Fractional Atomic Coordinates of **1** with Estimated Standard Deviations in Parentheses (Space Group *I2/m*, a = 9.428 (1) Å, b = 11.282 (2) Å, c = 11.272 (2) Å, β = 99.20)

atom	x/a	y/b	z/c
Ni	0.50000 (0)	0.60111 (7)	0.50000 (0)
Cl	0.50000 (0)	0.7910 (2)	0.50000 (0)
C1	0.4720 (6)	0.50000 (0)	0.6297 (5)
P	0.3793 (2)	0.50000 (0)	0.2561 (1)
Si	0.7138 (2)	0.50000 (0)	0.3315 (2)
C11	0.2088 (8)	0.50000 (0)	0.3053 (7)
C12	0.3735 (6)	0.3705 (5)	0.1611 (5)
C13	0.3735 (6)	0.6295 (5)	0.1611 (5)
C21	0.7181 (9)	0.50000 (0)	0.1648 (6)
C22	0.8157 (6)	0.6358 (5)	0.3890 (5)
C23	0.8157 (6)	0.3642 (5)	0.3890 (5)
H111	0.143 (5)	0.50000 (0)	0.230 (3)
H112	0.193 (4)	0.57021 (4)	0.351 (1)
H113	0.193 (4)	0.42979 (4)	0.351 (1)
H121	0.463	0.364	0.130
H122	0.295	0.378	0.095
H123	0.359	0.300	0.208
H131	0.463	0.636	0.130
H132	0.295	0.622	0.095
H133	0.359	0.700	0.208
H211	0.814 (3)	0.50000 (0)	0.144 (6)
H212	0.667 (2)	0.42979 (4)	0.132 (3)
H213	0.667 (2)	0.57021 (4)	0.132 (3)
H221	0.818	0.642	0.475
H222	0.769	0.705	0.350
H223	0.913	0.631	0.372
H231	0.818	0.358	0.475
H232	0.769	0.295	0.350
H233	0.913	0.369	0.372

Table III. Intra- and Interligand H···H Contacts Shorter Than 3 Å in **1**

H···H contacts	dist, Å	H···H contacts	dist, Å
	(1) Interligand		
H112···(H221)′	1.931	(H112)′···H221	1.931
H113···(H231)′	1.931	(H113)′···H231	1.931
	(2) Intraligand		
H121···H212	1.870	(H121)′···(H212)′	1.870
H131···H213	1.870	(H131)′···(H213)′	1.870

4.2. Steric Effects. In such a tightly bound complex, the 12 methyl groups in β position to the bridging carbon atoms should generate repulsive H···H contacts both inside each ylide ligand (intraligand contacts) and between opposite ligands (interligand contacts). The intra- and interligand contacts have opposite effects on the P–C–Si angles so that the equilibrium positions for this angle should minimize the global repulsion by equalizing the H···H contacts from intra- and interligand origins. The directions of the methyl hydrogens could be deduced from the crystal structure. The position of the hydrogen atoms was estimated first from the fractional atomic coordinates reported in Table II. Then, all C–H distances were scaled to 1.09 Å. With reference to Table II for the labeling of hydrogen atoms, Table III displays the eight close H···H contacts between hydrogens belonging to different substituents. Four interligand contacts, equivalent by symmetry, correspond to d_{H-H} = 1.931 Å, and four intraligand contacts, also equivalent, correspond to d_{H-H} = 1.870 Å. All other distances between hydrogens belonging to different substituents are over 3 Å. It is clear that there is a balance between intra- and interligand contacts, suggesting that the P–C–Si angles and possibly other geometrical parameters in the molecule have been influenced by sterical effects.

As a matter of fact, the interligand repulsions and, through the P–C–Si angles, the intraligand ones could be relieved through an increase of the C···C distance. Assuming the Ni–C bond lengths to remain constant, this trend would favor a decrease of both the Ni–C–Ni angle and the Ni–Ni distance. Combined with the electronic effects previously discussed, the steric effects could therefore push further the deformation of the metallacycle toward a still shorter metal–metal distance. Let us now try to obtain a rough quantitative estimate of the H···H repulsions, mainly to decide whether these repulsions have either a negligible or a significant or even prominent effect in determining the conformation of the metallacycle.

Modeling the H···H interactions from SCF calculations is not straightforward for several reasons. First, SCF calculations just account for the *repulsive* part of the nonbonding interactions. The attractive part, referred to as the "Hartree–Fock dispersion energy", could only be estimated by means of an appropriate CI calculation.[12] This treatment has not been carried out in the present work, but it can be shown that neighboring substituents are close enough in the molecule for the repulsive term to become largely dominant. Calculations on the intermolecular energy between two hydrogen molecules[13] have shown that the potential energy curve becomes repulsive for H···H distances shorter than 3.2–3.4 Å. The repulsive term then increases at an exponential rate and rapidly outstrips the attractive contribution of the dispersion energy. Calculations by Jorgensen on the structure of liquid *n*-butane[14] show that the CH_3···CH_3 radial distribution function at atmospheric pressure displays a maximum at $d_{C\cdots C}$ = 4.25 Å and rapidly decreases at shorter distances. The shortest C···C distances between carbons belonging to different substituents in **1** are 3.556 (intraligand) and 3.812 Å (interligand), which are clearly on the repulsive side of the interaction energy curve. The present calculations, aimed to provide no more than the order of magnitude of the H···H interaction energy, have been limited to the estimation of the repulsive part of this interaction. This part is expected to be largely dominant in the considered range of CH_3···CH_3 distances, but it should be corrected for the attractive contribution of the dispersion energy. The BSSE, which is another key factor in the calculation of intermolecular energies,[15] has been estimated using the counterpoise method of Boys and Bernardi.[3]

Modelization of the interacting fragments also requires care, since small repulsive interactions must be unambiguously picked out from the global interaction energy of the model fragments. In **1**, these fragments are four alternating $P(CH_3)_3$ and $Si(CH_3)_3$ substituents. An isolated, pyramidal $Si(CH_3)_3$ radical has little chemical meaning and might either influence the electronic structure of the methyl groups or generate unwanted interactions between P and Si. We have therefore replaced in our model Si by P, without modifying the geometry of the $SiMe_3$ substituent. One should then estimate the unwanted part of the fragment interaction energy, namely the repulsion between the phosphorus lone pairs. This repulsion is expected to outstrip the H···H interaction energy for intraligand model substituents due to the relatively small P···P distance (3.13 Å) and to the relative orientation of the lone pairs, deviating by no more than 30° from the P···P line. The two PMe_3 fragments mimicking the interligand interaction seem better suited to our goal because of the limited P···P interaction ($d_{P\cdots P}$ = 4.867 Å; direction of the lone pairs is 60° from the P···P line). We therefore restricted the model to two such PMe_3 fragments, assuming the intraligand H···H repulsions to be energetically equivalent to the interligand ones (see Table III). In spite of the long P···P distance, the calculation of the lone pair–lone lone pair repulsion remains necessary. It has been obtained from an ab initio SCF calculation on the H_3P···PH_3 model system, the hydrogens being oriented as are the carbons in Me_3P···PMe_3. Subtracting the sum of energies of the isolated fragments leads to the P···P repulsion energy. The same computational strategy applied to Me_3P···PMe_3 provides the total interaction energy, from which the P···P repulsion should be deduced in order to get the H···H contribution. The ab initio SCF energies obtained for the H_3P···PH_3 and Me_3P···PMe_3 model systems mimicking the interligand repulsion are displayed in Table IV. The H···H repulsion energy between two PMe_3 substituents attached to opposite carbons in the experimental (rhombus) conformation of the complex is estimated from the calculation

(12) Kollman, P. A.; Allen, L. C. *Chem. Rev.* **1972**, *72*, 283; *J. Chem. Phys.* **1970**, *52*, 5085.
(13) Kochanski, E. *Theor. Chim. Acta* **1975**, *39*, 339.
(14) Jorgensen, W. L. *J. Am. Chem. Soc.* **1981**, *103*, 4721.
(15) Urban, N.; Hobza, P. *Theor. Chim. Acta* **1975**, *36*, 207, 215.

Table IV. Ab Initio SCF Energies (hartrees) of the Model Systems Designed To Mimic the Interligand H···H Repulsion Energies in the Experimental (Rhombus) and Square Conformations of the Ni_2C_2 Metallacycle

	exptl conformation	square conformation
$H_3P{\cdots}PH_3$	−684.012 119	−684.011 565
$H_3P + PH_3$ (noninteracting)	−684.013 355	−684.013 355
including correction for BSSE	−684.013 520	−684.013 639
repulsion energy	0.001 401	0.002 074
$Me_3P{\cdots}PMe_3$	−917.988 877	−917.977 519
$Me_3P + PMe_3$ (noninteracting)	−917.994 890	−917.994 890
including correction for BSSE	−917.996 622	−917.997 022
tot. repulsion	0.007 745	0.019 503
H···H repulsion[a]	0.006 344	0.017 429
tot. interligand H···H repulsion[b]	0.012 688	0.034 858
tot. H···H repulsion[c]	0.025 376	0.047 546

[a] Between two interligand substituents. [b] Twice the value computed in footnote *a*. [c] Assuming the intraligand repulsion energy to be identical to the interligand one in the experimental conformation. This estimate of the intraligand repulsion energy (0.012 688 hartree) is transferred without change to the square conformation, since the orientation of the PMe_3 fragments has not been modified.

to be 16.6 kJ·mol^{-1}. Assuming the repulsion to be identical between each pair of interacting substituents either inter- or intraligand, the total repulsion energy for the complex should be 66 kJ·mol^{-1}.[16]

Another important assessment to be obtained is the variation of the steric repulsion when the metallacycle is distorted into the square conformation. The interligand repulsion in that conformation has been estimated by just compelling the PMe_3 fragments to come closer by 0.36 Å, this value corresponding to the decrease of the C···C distance. The interligand H···H repulsion between two PMe_3 fragments was then computed to be 45.7 kJ·mol^{-1}. Since no reorientation of the PMe_3 fragments has been allowed for, the value of 16.6 kJ·mol^{-1}, assumed for intraligand H···H repulsion, was retained for the square conformation, leading to an estimate of 125 kJ·mol^{-1} for the overall repulsion energy in the complex.

The steric barrier against a deformation of the metallacycle into the square conformation could therefore reach the order of magnitude of 60 kJ·mol^{-1}. This value may however appear modest with regard to the energy barrier ascribed to purely electronic effects. If we start from the minimum of the EH potential energy curve derived for **2**, the energy rise associated with a 16.5° decrease of the C–Ni–C angle reaches 100 kJ·mol^{-1} (Figure 7). Even if the steepness of the potential energy curve associated with purely electronic effects was to be confirmed by ab initio calculations, the steric contribution is susceptible to somewhat displace the equilibrium position toward higher values of the C–Ni–C angles, i.e. toward a shorter Ni–Ni distance. An elongation of the nickel–carbon bond could also be considered as a possible consequence of the steric congestion even though this distance in **1** appears very short (1.906 Å).

Apart from the amide-bridged nickel dimer $[Ni(NPh_2)_2]_2$ discussed above and representing another example of a sterically crowded dimer of Ni(II) with a very short metal–metal bond (2.327 Å),[9] let us finally mention the case of $\{NiPMe_3[\mu\text{-}P(t\text{-}Bu)_2]\}_2$ (**10**), a dimer of nickel(I) characterized by Jones et al.[17] It has been acknowledged in that report that the *tert*-butyl substituents of the bridging phosphido groups are at the origin of nonbonded H···H contacts between the methyl groups of neighboring substituents. Studies using space filling CPK models have suggested that steric hindrance was at the origin of the unexpected planarity of the Ni_2P_2 metallacycle. Since the space filling capacity of the *t*-Bu groups is similar to that of PMe_3 and $SiMe_3$ substituents, it may be thought that balanced intra- and interligand repulsions are developing in **10** as in **2**, eventually leading to a deformation of the metallacycle. The structure of **10** seems to support this hypothesis: the planar Ni_2P_2 metallacycle is strongly rhombic with a Ni–P–Ni angle of 66.2° and a very short Ni–Ni distance of 2.375 Å.[17]

Acknowledgment. The ab initio SCF and part of the EH calculations have been carried out on the IBM-3090/200 computer of the Centre de Calcul de Strasbourg, through a grant of computer time from the CNRS.

Registry No. 1, 127518-58-5.

(16) One should notice here that this conformation of the methyl hydrogens deduced from the X-ray structure (Table II) is far from minimizing the repulsive effects, either intraligand or interligand, between opposite substituents. Appropriate rotations of the methyl groups around the P–C or Si–C axes increase the H···H distances from ~1.9 to 2.4–2.7 Å and reduce the associated repulsion energy from 66 to 17.5 kJ·mol^{-1}. The experimental conformation is nevertheless more stable due to an optimization of the H···H contacts *inside each* PMe_3 *or* $SiMe_3$ *substituent*.

(17) Jones, R. A.; Stuart, A. L.; Atwood, J. L.; Hunter, W. E.; Rogers, R. D. *Organometallics* **1982**, *1*, 1721.